1750–2011 (from the model ensemble of Orr et al., (2005) until 1994, plus an additional 40 PgC from estimates in Table 6.4 for 1995–2011), a mean anthropogenic CO_2 sink of 2.1 ± 0.6 PgC yr^{-1} for 1990–1999 (Le Quéré et al., 2013) and a decadal trend of 0.14 PgC yr^{-1} per decade for 1990–2009 (Wanninkhof et al., 2013). Therefore, although the ocean models do not reproduce all the details of the regional structure and changes in air–sea CO_2 fluxes, their globally integrated ocean CO_2 sink and decadal rate of change of this sink is in good agreement with the available observations.

Sensitivity of modelled air–sea fluxes to climate. The relationship between air–sea CO_2 flux and climate is strongly dependent on the oceanic region and on the time scale. Ocean carbon cycle models of the type used in AR5 estimate a reduction in cumulative ocean CO_2 uptake of 1.6 to 5.4 PgC over the period 1959–2008 (1.5 to 5.4%) in response to climate change and variability compared to simulations with no changes in climate (Figure 6.14), partly due to changes in the equatorial Pacific and to changes in the Southern Ocean. The only observation-based estimate available to evaluate the climate response of the global air–sea CO_2 flux is from Park et al. (2010), which is at the low end of the model estimate for the past two decades (Table 6.4). However, this estimate does not include the nonlinear effects of changes in ocean circulation and warming on the global air–sea CO_2 flux, which could amplify the response of the ocean CO_2 sink to climate by 20 to 30% (Le Quéré et al., 2010; Zickfeld et al., 2011).

Processes missing in ocean models. The most important processes missing in ocean carbon cycle models used in the AR5 are those representing explicitly small-scale physical circulation (e.g., eddies, brine formation), which are parameterised in models. These processes have an important influence on the vertical transport of water, heat, salt and carbon (Loose and Schlosser, 2011; Sallée et al., 2012). In particular, changes in vertical transport in the Southern Ocean are thought to explain part of the changes in atmospheric CO_2 between glacial and interglacial conditions, a signal that is not entirely reproduced by models (Section 6.2) suggesting that the sensitivity of ocean models could be underestimated.

Processes related to marine ecosystems in global ocean models are also limited to the simulation of lower trophic levels, with crude parameterizations for sinking processes, bacterial and other loss processes at the surface and in the ocean interior and their temperature dependence (Kwon et al., 2009). Projected changes in carbon fluxes from the response of marine ecosystems to changes in temperature (Beaugrand et al., 2010), ocean acidification (Riebesell et al., 2009) (see Glossary) and pressure from fisheries (Pershing et al., 2010) are all considered potentially important, though not yet quantified. Several processes have been specifically identified that could lead to changes in the ocean CO_2 sink, in particular the temperature effects on marine ecosystem processes (Riebesell et al., 2009; Taucher and Oschlies, 2011) and the variable nutrient ratios induced by ocean acidification or ecosystem changes (Tagliabue et al., 2011). Coastal ocean processes are also poorly represented in global and may influence the ocean CO_2 sink. Nevertheless, the fit of ocean model results to the integrated CO_2 sink and decadal trends discussed above suggest that, up to now, the missing processes have not had a dominant effect on ocean CO_2 beyond the limits of the uncertainty of the data.

6.3.2.6 Land Carbon Dioxide Sink

6.3.2.6.1 Global residual land sink and atmosphere-to-land carbon dioxide flux

The residual land CO_2 sink, that is, the uptake of CO_2 in ecosystems excluding the effects of land use change, is 1.5 ± 1.1, 2.6 ± 1.2 and 2.6 ± 1.2 PgC yr^{-1} for the 1980s, 1990s and 2000s, respectively (Table 6.1). After including the net land use change emissions, the atmosphere-to-land flux of CO_2 (Table 6.1) corresponds to a net sink of CO_2 by all terrestrial ecosystems. This sink has intensified globally from a neutral CO_2 flux of 0.1 ± 0.8 PgC yr^{-1} in the 1980s to a net CO_2 sink of 1.1 ± 0.9 PgC yr^{-1} and 1.5 ± 0.9 PgC yr^{-1} during the 1990s and 2000s, respectively (Table 6.1; Sarmiento et al., 2010). This growing land sink is also supported by an atmospheric inversion (Gurney and Eckels, 2011) and by process-based models (Le Quéré et al., 2009).

6.3.2.6.2 Regional atmosphere-to-land carbon dioxide fluxes

The results from atmospheric CO_2 inversions, terrestrial ecosystem models and forest inventories consistently show that there is a large net CO_2 sink in the northern extratropics, albeit the very limited availability of observations in the tropics (Jacobson et al., 2007; Gurney and Eckels, 2011; Pan et al., 2011). Inversion estimates of atmosphere–land CO_2 fluxes show net atmosphere-to-land CO_2 flux estimates ranging from neutral to a net source of 0.5 to 1.0 PgC yr^{-1} (Jacobson et al., 2007; Gurney and Eckels, 2011) (Figure 6.15). However, Stephens et al. (2007) selected from an ensemble of inversion models those that were consistent with independent aircraft cross-validation data, and constrained an atmosphere-to-land CO_2 flux of 0.1 ± 0.8 PgC yr^{-1} during the period 1992–1996, and a NH net CO_2 sink of 1.5 ± 0.6 PgC yr^{-1}. These results shows that after subtracting emissions from land use change, tropical land ecosystems might also be large CO_2 sinks.

Based on repeated forest biomass inventory data, estimated soil carbon changes, and CO_2 emissions from land use change from the bookkeeping method of Houghton et al. (2012), Pan et al. (2011) estimated a global forest carbon accumulation of 0.5 ± 0.1 PgCyr^{-1} in boreal forests, and of 0.8 ± 0.1 PgC yr^{-1} in temperate forests for the period 2000–2007. Tropical forests were found to be near neutral with net emissions from land use change being compensated by sinks in established tropical forests (forests not affected by land use change), therefore consistent with the Stephens et al. (2007) inversion estimate of tropical atmosphere–land CO_2 fluxes.

Since AR4, a number of studies have compared and attempted to reconcile regional atmosphere-to-land CO_2 flux estimates from multiple approaches and so providing further spatial resolution of the regional contributions of carbon sources and sinks (Table 6.6). A synthesis of regional contributions estimated a 1.7 PgC yr^{-1} sink in the NH regions above 20°N with consistent estimates from terrestrial models and inventories (uncertainty: ±0.3 PgC yr^{-1}) and atmospheric CO_2 inversions (uncertainty: ±0.7 PgC yr^{-1}) (Ciais et al., 2010).

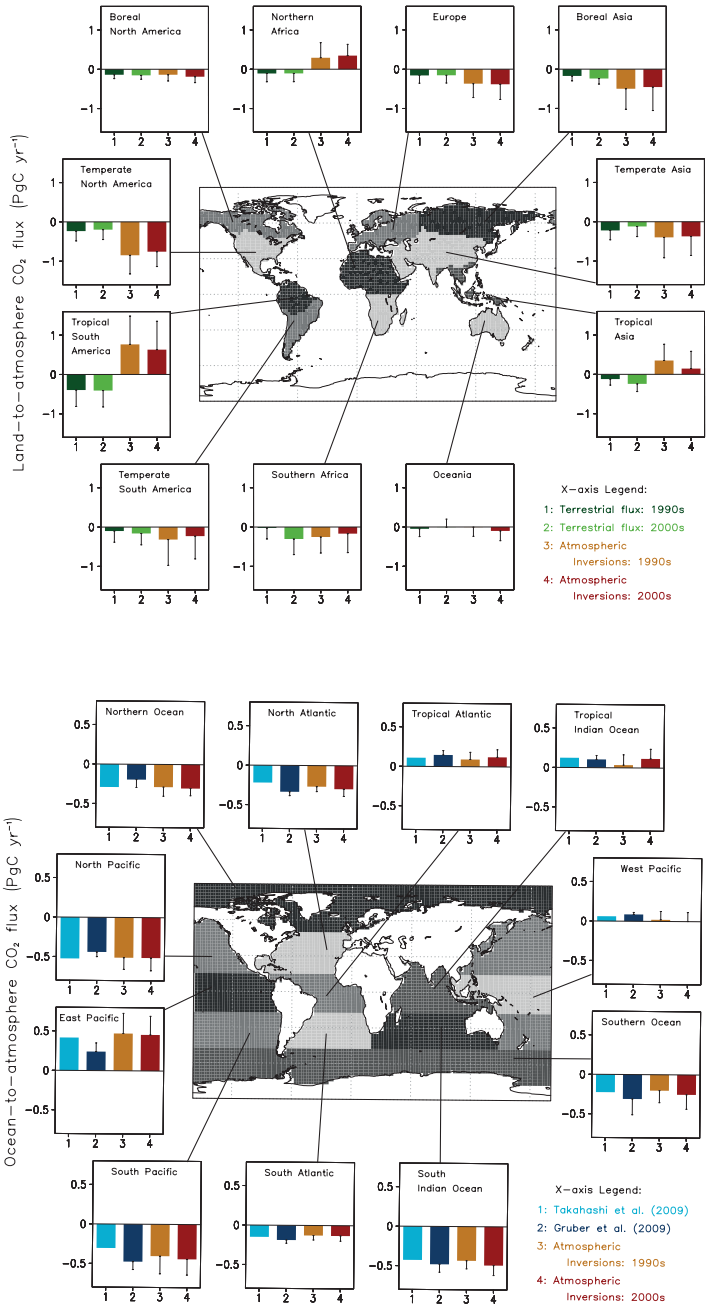

Figure 6.15 | (Top) Bar plots showing decadal average CO_2 fluxes for 11 land regions (1) as estimated by 10 different atmospheric CO_2 inversions for the 1990s (yellow) and 2000s (red) (Peylin et al., 2013; data source: http://transcom.lsce.ipsl.fr/), and (2) as simulated by 10 dynamic vegetation models (DGVMs) for the 1990s (green) and 2000s (light green) (Piao et al., 2013; data source: http://www-lscedods.cea.fr/invsat/RECCAP/). The divisions of land regions are shown in the map. (Bottom) Bar plots showing decadal average CO_2 fluxes for 11 ocean regions (1) as estimated by 10 different atmospheric CO_2 inversions for the 1990s (yellow) and 2000s (red) (data source: http://transcom.lsce.ipsl.fr/), (2) inversion of contemporary interior ocean carbon measurements using 10 ocean transport models (dark blue) (Gruber et al., 2009) and (3) surface ocean pCO_2 measurements based air-sea exchange climatology (Takahashi et al., 2009). The divisions of 11 ocean regions are shown in the map.

Table 6.6 | Regional CO_2 budgets using top-down estimates (atmospheric inversions) and bottom-up estimates (inventory data, biogeochemical modelling, eddy-covariance), excluding fossil fuel emissions. A positive sign indicates a flux from the atmosphere to the land (i.e., a land sink).

Region	CO_2 Sink (PgC yr^{-1})	Uncertainty[a]	Period	Reference
Artic Tundra	0.1	±0.3[b]	2000–2006	McGuire et al. (2012)
Australia	0.04	±0.03	1990–2009	Haverd et al. (2013)
East Asia	0.25	±0.1	1990–2009	Piao et al. (2012)
Europe	0.9	±0.2	2001–2005	Luyssaert et al. (2012)
North America	0.6	±0.02	2000–2005	King et al. (2012)
Russian Federation	0.6	–0.3 to –1.3	1990–2007	Dolman et al. (2012)
South Asia	0.15	±0.24	2000–2009	Patra et al. (2013)
South America	–0.3	±0.3	2000–2005	Gloor et al. (2012)

Notes:

[a] One standard deviation from mean unless indicated otherwise.

[b] Based on range provided.

6.3.2.6.3 Interannual variability in atmosphere-to-land carbon dioxide fluxes

The interannual variability of the residual land sink shown in Figures 6.12 and 6.16 accounts for most of the interannual variability of the atmospheric CO_2 growth rate (see Section 6.3.2.3). Atmospheric CO_2 inversion results suggest that tropical land ecosystems dominate the global CO_2 variability, with positive anomalies during El Niño episodes (Bousquet et al., 2000; Rödenbeck et al., 2003; Baker et al., 2006), which is consistent with the results of one inversion of atmospheric ^{13}C and CO_2 measurements (Rayner et al., 2008). A combined El Niño-Southern Oscillation (ENSO)–Volcanic index time series explains 75% of the observed variability (Raupach et al., 2008). A positive phase of ENSO (El Niño, see Glossary) is generally associated with enhanced land CO_2 source, and a negative phase (La Niña) with enhanced land CO_2 sink (Jones and Cox, 2001; Peylin et al., 2005). Observations from eddy covariance networks suggest that interannual carbon flux variability in the tropics and temperate regions is dominated by precipitation, while boreal ecosystem fluxes are more sensitive to temperature and shortwave radiation variation (Jung et al., 2011), in agreement with the results from process-based terrestrial ecosystem models (Piao et al., 2009a). Terrestrial biogeochemical models suggest that interannual net biome productivity (NBP) variability is dominated by GPP (see Glossary) rather than terrestrial ecosystem respiration (Piao et al., 2009b; Jung et al., 2011).

6.3.2.6.4 Carbon fluxes from inland water

Global analyses estimate that inland waters receive about 1.7 to 2.7 PgC yr^{-1} emitted by soils to rivers headstreams, of which, 0.2 to 0.6 PgC yr^{-1} is buried in aquatic sediments, 0.8 to 1.2 PgC yr^{-1} returns to the atmosphere as CO_2, and 0.9 PgC yr^{-1} is delivered to the ocean (Cole et al., 2007; Battin et al., 2009; Aufdenkampe et al., 2011). Estimates of the transport of carbon from land ecosystems to the coastal ocean by rivers are ~0.2 PgC yr^{-1} for Dissolved Organic Carbon (DOC), 0.3 PgC yr^{-1} for Dissolved Inorganic Carbon (DIC), and 0.1 to 0.4 PgC yr^{-1} for Particulate Organic Carbon (POC) (Seitzinger et al., 2005; Syvitski et al., 2005; Mayorga et al., 2010). For the DIC fluxes, only about two-thirds of it originates from atmospheric CO_2 and the rest of the carbon is supplied by weathered carbonate rocks (Suchet and Probst, 1995; Gaillardet et al., 1999; Oh and Raymond, 2006; Hartmann et al., 2009). Regional DIC concentrations in rivers has increased during the Industrial Era (Oh and Raymond, 2006; Hamilton et al., 2007; Perrin et al., 2008). Agricultural practices coupled with climate change can lead to large increases in regional scale DIC export in watersheds with a large agricultural footprint (Raymond et al., 2008). Furthermore, regional urbanization also elevates DIC fluxes in rivers (Baker et al., 2008; Barnes and Raymond, 2009), which suggests that anthropogenic activities have contributed a significant portion of the annual global river DIC flux to the ocean.

Land clearing and management are thought to produce an acceleration of POC transport, much of which is trapped in alluvial and colluvial deposition zones, lakes, reservoirs and wetlands (Stallard, 1998; Smith et al., 2001b; Syvitski et al., 2005). Numerous studies have demonstrated an increase in the concentration of DOC in rivers in the northeastern United States and northern/central Europe over the past two to four decades (Worrall et al., 2003; Evans et al., 2005; Findlay, 2005; Monteith et al., 2007; Lepistö et al., 2008). Owing to the important role of wetlands in DOC production, the mobilization of DOC due to human-induced changes in wetlands probably represents an important cause of changes in global river DOC fluxes to date (Seitzinger et al., 2005), although a global estimate of this alteration is not available. A robust partitioning between natural and anthropogenic carbon fluxes in freshwater systems is not yet possible, nor a quantification of the ultimate fate of carbon delivered by rivers to the coastal and open oceans.

6.3.2.6.5 Processes driving terrestrial atmosphere-to-land carbon dioxide fluxes

Assessment of experimental data, observations and model results suggests that the main processes responsible for the residual land sink include the CO_2 fertilisation effect on photosynthesis (see Box 6.3), nitrogen fertilisation by increased deposition (Norby, 1998; Thornton et al., 2007; Bonan and Levis, 2010; Zaehle and Dalmonech, 2011) and climate effects (Nemani et al., 2003; Gloor et al., 2009). It is *likely* that reactive nitrogen deposition over land currently increases natural CO_2 in particular in forests, but the magnitude of this effect varies between regions (Norby, 1998; Thornton et al., 2007; Bonan and Levis, 2010; Zaehle and Dalmonech, 2011). Processes responsible for the net atmosphere-to-land CO_2 sink on terrestrial ecosystems include, in addition, forest regrowth and afforestation (Myneni et al., 2001;

Box 6.3 | The Carbon Dioxide Fertilisation Effect

Elevated atmospheric CO_2 concentrations lead to higher leaf photosynthesis and reduced canopy transpiration, which in turn lead to increased plant water use efficiency and reduced fluxes of surface latent heat. The increase in leaf photosynthesis with rising CO_2, the so-called CO_2 fertilisation effect, plays a dominant role in terrestrial biogeochemical models to explain the global land carbon sink (Sitch et al., 2008), yet it is one of most unconstrained process in those models.

Field experiments provide a direct evidence of increased photosynthesis rates and water use efficiency (plant carbon gains per unit of water loss from transpiration) in plants growing under elevated CO_2. These physiological changes translate into a broad range of higher plant carbon accumulation in more than two-thirds of the experiments and with increased net primary productivity (NPP) of about 20 to 25% at double CO_2 from pre-industrial concentrations (Ainsworth and Long, 2004; Luo et al., 2004, 2006; Nowak et al., 2004; Norby et al., 2005;Canadell et al., 2007a; Denman et al., 2007; Ainsworth et al., 2012; Wang et al., 2012a). Since the AR4, new evidence is available from long-term Free-air CO_2 Enrichment (FACE) experiments in temperate ecosystems showing the capacity of ecosystems exposed to elevated CO_2 to sustain higher rates of carbon accumulation over multiple years (Liberloo et al., 2009; McCarthy et al., 2010; Aranjuelo et al., 2011; Dawes et al., 2011; Lee et al., 2011; Zak et al., 2011). However, FACE experiments also show the diminishing or lack of CO_2 fertilisation effect in some ecosystems and for some plant species (Dukes et al., 2005; Adair et al., 2009; Bader et al., 2009; Norby et al., 2010; Newingham et al., 2013). This lack of response occurs despite increased water use efficiency, also confirmed with tree ring evidence (Gedalof and Berg, 2010; Peñuelas et al., 2011).

Nutrient limitation is hypothesized as primary cause for reduced or lack of CO_2 fertilisation effect observed on NPP in some experiments (Luo et al., 2004; Dukes et al., 2005; Finzi et al., 2007; Norby et al., 2010). Nitrogen and phosphorus are *very likely* to play the most important role in this limitation of the CO_2 fertilisation effect on NPP, with nitrogen limitation prevalent in temperate and boreal ecosystems, and phosphorus limitation in the tropics (Luo et al., 2004; Vitousek et al., 2010; Wang et al., 2010a; Goll et al., 2012). Micronutrients interact in diverse ways with other nutrients in constraining NPP such as molybdenum and phosphorus in the tropics (Wurzburger et al., 2012). Thus, with *high confidence*, the CO_2 fertilisation effect will lead to enhanced NPP, but significant uncertainties remain on the magnitude of this effect, given the lack of experiments outside of temperate climates.

Pacala et al., 2001; Houghton, 2010; Bellassen et al., 2011; Williams et al., 2012a), changes in forest management and reduced harvest rates (Nabuurs et al., 2008).

Process attribution of the global land CO_2 sink is difficult due to limited availability of global data sets and biogeochemical models that include all major processes. However, regional studies shed light on key drivers and their interactions. The European and North American carbon sinks are explained by the combination of forest regrowth in abandoned lands and decreased forest harvest along with the fertilisation effects of rising CO_2 and nitrogen deposition (Pacala et al., 2001; Ciais et al., 2008; Sutton et al., 2008; Schulze et al., 2010; Bellassen et al., 2011; Williams et al., 2012a). In the tropics, there is evidence from forest inventories that increasing forest growth rates are not explained by the natural recovery from disturbances, suggesting that increasing atmospheric CO_2 and climate change play a role in the observed sink in established forests (Lewis et al., 2009; Pan et al., 2011). There is also recent evidence of tropical nitrogen deposition becoming more notable although its effects on the net carbon balance have not been assessed (Hietz et al., 2011).

The land carbon cycle is very sensitive to climate changes (e.g., precipitation, temperature, diffuse vs. direct radiation), and thus the changes in the physical climate from increasing GHGs as well as in the diffuse fraction of sunlight are *likely* to be causing significant changes in the carbon cycle (Jones et al., 2001; Friedlingstein et al., 2006; Mercado et al., 2009). Changes in the climate are also associated with disturbances such as fires, insect damage, storms, droughts and heat waves which are already significant processes of interannual variability and possibly trends of regional land carbon fluxes (Page et al., 2002; Ciais et al., 2005; Chambers et al., 2007; Kurz et al., 2008b; Clark et al., 2010; van der Werf et al., 2010; Lewis et al., 2011) (see Section 6.3.2.2).

Warming (and possibly the CO_2 fertilisation effect) has also been correlated with global trends in satellite greenness observations, which resulted in an estimated 6% increase of global NPP, or the accumulation of 3.4 PgC on land over the period 1982–1999 (Nemani et al., 2003). This enhanced NPP was attributed to the relaxation of climatic constraints to plant growth, particularly in high latitudes. Concomitant to the increased of NPP with warming, global soil respiration also increased between 1989 and 2008 (Bond-Lamberty and Thomson, 2010), reducing the magnitude of the net land sink. A recent study suggests a declining NPP trend over 2000–2009 (Zhao and Running, 2010) although the model used to reconstruct NPP trends from satellite observation has not been widely accepted (Medlyn, 2011; Samanta et al., 2011).

6.3.2.6.6 Model evaluation of global and regional terrestrial carbon balance

Evaluation of global process-based land carbon models was performed against ground and satellite observations including (1) measured CO_2

fluxes and carbon storage change at particular sites around the world, in particular sites from the Fluxnet global network (Baldocchi et al., 2001; Jung et al., 2007; Stöckli et al., 2008; Schwalm et al., 2010; Tan et al., 2010), (2) observed spatio-temporal change in leaf area index (LAI) (Lucht et al., 2002; Piao et al., 2006) and (3) interannual and seasonal change in atmospheric CO_2 (Randerson et al., 2009; Cadule et al., 2010).

Figure 6.16 compares the global land CO_2 sink driven by climate change and rising CO_2 as simulated by different process based carbon cycle models (without land use change), with the residual land sink computed as the sum of fossil fuel and cement emissions and land use change emissions minus the sum of CO_2 growth rate and ocean sink (Le Quéré et al., 2009; Friedlingstein et al., 2010). Although these two quantities are not the same, the multi-model mean reproduces well the trend and interannual variability of the residual land sink which is dominated by climate variability and climate trends and CO_2, respectively, both represented in models (Table 6.7). Limited availability of *in situ* measurements, particularly in the tropics, limits the progress towards reducing uncertainty on model parameterizations.

Regional and local measurements can be used to evaluate and improve global models. Regionally, forest inventory data show that the forest carbon sink density over Europe is of –89 ± 19 gC m^{-2} yr^{-1}, which is compatible with model estimates with afforestation (–63 gC m^{-2} yr^{-1}; Luyssaert et al., 2010), while modelled NPP was 43% larger than the inventory estimate. In North America, the ability of 22 terrestrial carbon cycle models to simulate the seasonal cycle of land–atmosphere CO_2 exchange from 44 eddy covariance flux towers was poor with a difference between observations and simulations of 10 times the observational uncertainty (Schwalm et al., 2010). Model shortcomings included spring phenology, soil thaw, snow pack melting and lag responses to extreme climate events (Keenan et al., 2012). In China, the magnitude of the carbon sink estimated by five terrestrial ecosystem models (–0.22 to –0.13 PgC yr^{-1}) was comparable to the observation-based estimate (–0.18 ± 0.73 PgC yr^{-1}; Piao et al., 2009a), but modelled interannual variation was weakly correlated to observed regional land–atmosphere CO_2 fluxes (Piao et al., 2011).

Sensitivity of the terrestrial carbon cycle to rising atmospheric carbon dioxide. An inter-comparison of 10 process-based models showed increased NPP by 3% to 10% over the last three decades, during which CO_2 increased by ~50 ppm (Piao et al., 2013). These results are consistent within the broad range of responses from experimental studies (see Box 6.3). However, Hickler et al. (2008) suggested that currently available FACE results (largely from temperate regions) are not applicable to vegetation globally because there may be large spatial heterogeneity in vegetation responses to CO_2 fertilisation.

Table 6.7 | Estimates of the land CO_2 sink from process-based terrestrial ecosystem models driven by rising CO_2 and by changes in climate. The land sink simulated by these models is close to but not identical to the terrestrial CO_2 sink from Table 6.1 because the models calculate the effect of CO_2 and climate over managed land, and many do not include nitrogen limitation and disturbances.

Model Name	Nitrogen Limitation	Natural Fire CO_2 Emissions	1980–1989	1990–1999	2000–2009
	(Yes/No)	(Yes/No)	PgC yr^{-1}	PgC yr^{-1}	PgC yr^{-1}
CLM4C[b,c]	No	Yes	1.98	2.11	2.64
CLM4CN[b,c]	Yes	Yes	1.27	1.25	1.67
Hyland[d]	No	No	2.21	2.92	3.99
LPJ[e]	No	Yes	1.14	1.90	2.60
LPJ_GUESS[f]	No	Yes	1.15	1.54	2.07
OCN[g]	Yes	No	1.75	2.18	2.36
ORC[h]	No	No	2.08	3.05	3.74
SDGVM[i]	Yes	Yes	1.25	1.95	2.30
TRIFFID[j]	No	No	1.85	2.52	3.00
VEGAS[k]	No	No	1.40	1.68	1.89
Average[a]			1.61 ± 0.65	2.11 ± 0.93	2.63 ± 1.22

Notes:

[a] Average of all models ±90% confidence interval.
[b] Oleson et al. (2010).
[c] Lawrence et al. (2011).
[d] Levy et al. (2004).
[e] Sitch et al. (2003).
[f] Smith et al. (2001a).
[g] Zaehle and Friend (2010).
[h] Krinner et al. (2005).
[i] Woodward and Lomas (2004).
[j] Cox (2001).
[k] Zeng (2003).

All of these models run are forced by rising CO_2 concentration and time-varying historical reconstructed weather and climate fields using the same protocol from the TRENDY project (Piao et al., 2013). (http://www.globalcarbonproject.org/global/pdf/DynamicVegetationModels.pdf).

CLM4C = Community Land Model for Carbon; CLM4CN = Community Land Model for Carbon–Nitrogen; GUESS = General Ecosystem Simulator; LPJ = Lund-Potsdam-Jena Dynamic Global Vegetation Model; OCN = Cycling of Carbon and Nitrogen on land, derived from ORCHIDEE model; ORC = ORCHIDEE, ORganizing Carbon and Hydrology in Dynamic EcosystEms model; SDGVM = Sheffield Dynamic Global Vegetation Model; TRIFFID = Top-down Representation of Interactive Foliage and Flora Including Dynamics; VEGAS = VEgetation-Global-Atmosphere-Soil terrestrial carbon cycle model.

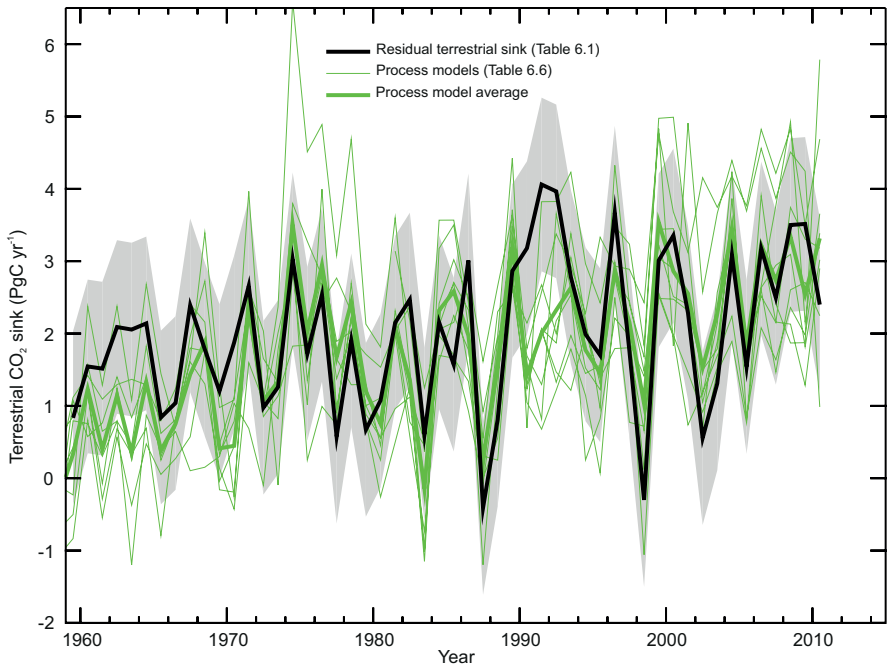

Figure 6.16 | The black line and gray shading represent the estimated value of the residual land sink (PgC yr^{-1}) and its uncertainty from Table 6.1, which is calculated from the difference between emissions from fossil fuel and land use change plus emissions from net land use change, minus the atmospheric growth rate and the ocean sink. The atmosphere-to-land flux simulated by process land ecosystem models from Table 6.7 are shown in thin green, and their average in thick green. A positive atmosphere-to-land flux represents a sink of CO_2. The definition of the atmosphere-to-land flux simulated by these models is close to but not identical to the residual land sink from Table 6.1 (see Table 6.7).

Sensitivity of terrestrial carbon cycle to climate trends and variability. Warming exerts a direct control on the net land–atmosphere CO_2 exchange because both photosynthesis and respiration are sensitive to changes in temperature. From estimates of interannual variations in the residual land sink, 1°C of positive global temperature anomaly leads to a decrease of 4 PgC yr^{-1} of the global land CO_2 sink (Figure 6.17). This observed interannual response is close to the response of the models listed in Table 6.7 (–3.5 ± 1.5 PgC $yr^{-1}°C^{-1}$ in Piao et al., 2013), albeit individual models show a range going from –0.5 to –6.2 PgC yr^{-1} $°C^{-1}$. The sensitivity of atmospheric CO_2 concentration to century scale temperature change was estimated at about 3.6 to 45.6 PgC $°C^{-1}$ (or 1.7 to 21.4 ppm CO_2 $°C^{-1}$) using the ice core observed CO_2 drop during the Little Ice Age (see Section 6.2; Frank et al., 2010).

Terrestrial carbon cycle models used in AR5 generally underestimate GPP in the water limited regions, implying that these models do not correctly simulate soil moisture conditions, or that they are too sensitive to changes in soil moisture (Jung et al., 2007). Most models (Table 6.7) estimated that the interannual precipitation sensitivity of the global land CO_2 sink to be higher than that of the observed residual land sink (–0.01 PgC yr^{-1} mm^{-1}; Figure 6.17).

Processes missing in terrestrial carbon cycle models. First, many models do not explicitly take into account the various forms of disturbances or ecosystem dynamics: migration, fire, logging, harvesting, insect outbreaks and the resulting variation in forest age structure which is known to affect the net carbon exchange (Kurz et al., 2008c; Bellassen et al., 2010; Higgins and Harte, 2012). Second, many key processes relevant to decomposition of carbon are missing in models (Todd-Brown et al., 2012), and particularly for permafrost carbon and for carbon in boreal and tropical wetlands and peatlands, despite the large amount of carbon stored in these ecosystems and their vulnerability to warming and land use change (Tarnocai et al., 2009; Hooijer et al., 2010; Page et al., 2011). However, progress has been made (Wania et al., 2009; Koven et al., 2011; Schaefer et al., 2011). Third, nutrient dynamics are taken into account only by few models despite the fact it is well established that nutrient constrains NPP and nitrogen deposition enhances NPP (Elser et al., 2007; Magnani et al., 2007; LeBauer and Treseder, 2008); see Section 6.3.2.6.5. Very few models have phosphorus dynamics (Zhang et al., 2011; Goll et al., 2012). Fourth, the negative effects of elevated tropospheric ozone on NPP have not been taken into account by most current carbon cycle models (Sitch et al., 2007). Fifth, transfer of radiation, water and heat in the vegetation–soil–atmosphere continuum are treated very simply in the global ecosystem models. Finally, processes that transport carbon at the surface (e.g., water and tillage erosion; Quinton et al., 2010) and human managements including fertilisation and irrigation (Gervois et al., 2008) are poorly or not represented at all. Broadly, models are still at their early stages in dealing with land use, land use change and forestry.

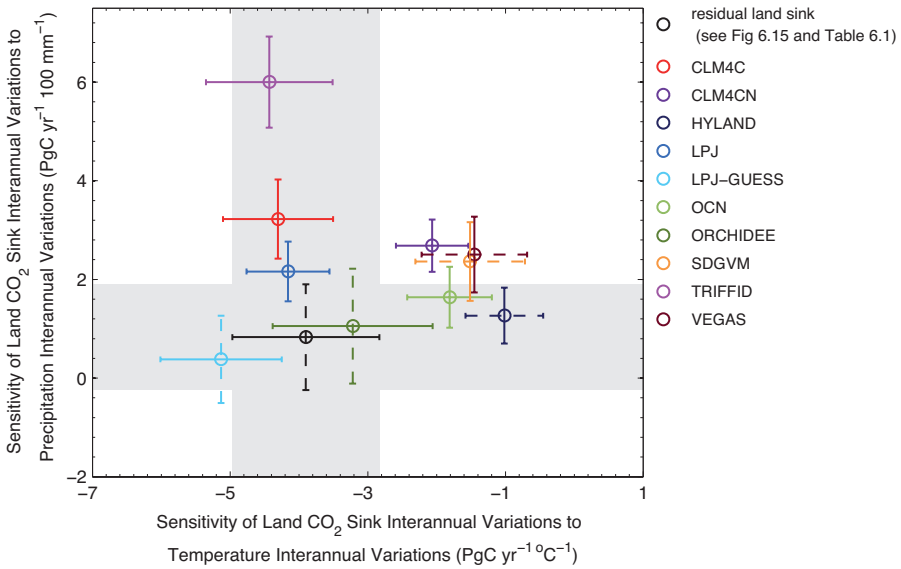

Figure 6.17 | The response of interannual land CO_2 flux anomaly to per 1°C interannual temperature anomaly and per 100 mm interannual precipitation anomaly during 1980–2009. Black circles show climate sensitivity of land CO_2 sink estimated from the residual land sink (see Figure 6.15 and Table 6.1), which is the sum of fossil fuel and cement emissions and land use change emissions minus the sum of observed atmospheric CO_2 growth rate and modeled ocean sink sink (Le Quéré et al., 2009; Friedlingstein and Prentice, 2010). Coloured circles show land CO_2 sink estimated by 10 process-based terrestrial carbon cycle models (CLM4C (Community Land Model for Carbon), CLM4CN (Community Land Model for Carbon–Nitrogen), HYLAND (HYbrid LAND terrestrial ecosystem model), LPJ (Lund-Potsdam-Jena Dynamic Global Vegetation Model), LPJ–GUESS (LPJ–General Ecosystem Simulator, OCN (Cycling of Carbon and Nitrogen on land, derived from ORCHIDEE model), ORCHIDEE (ORganizing Carbon and Hydrology in Dynamic EcosystEms model), SDGVM (Sheffield Dynamic Global Vegetation Model), TRIFFID (Top-down Representation of Interactive Foliage and Flora Including Dynamics) and VEGAS (terrestrial vegetation and carbon model)). Error bars show standard error of the sensitivity estimates. Dashed error bars indicate the estimated sensitivity by the regression approach is statistically insignificant ($P > 0.05$). Grey area denoted the area bounded by the estimated climate sensitivity of the residual land sink ± the standard error of the estimated climate sensitivity of the residual land sink. The sensitivity of land CO_2 sink interannual variations to interannual variations of temperature (or precipitation) is estimated as the regression coefficient of temperature (or precipitation) in a multiple regression of detrended anomaly of land CO_2 sink against detrended anomaly of annual mean temperature and annual precipitation.

6.3.3 Global Methane Budget

AR5 is the first IPCC assessment report providing a consistent synthesis of the CH_4 budget per decade using multiple atmospheric CH_4 inversion models (top-down) and process-based models and inventories (bottom-up). Table 6.8 shows the budgets for the decades of 1980s, 1990s and 2000s. Uncertainties on emissions and sinks are listed using minimum and maximum of each published estimate for each decade. Bottom-up approaches are used to attribute decadal budgets to individual processes emitting CH_4 (see Section 6.1.1.2 for a general overview). Top-down inversions provide an atmospheric-based constraint mostly for the total CH_4 source per region, and the use of additional observations (e.g., isotopes) allows inferring emissions per source type. Estimates of CH_4 sinks in the troposphere by reaction with tropospheric OH, in soils and in the stratosphere are also presented. Despite significant progress since the AR4, large uncertainties remain in the present knowledge of the budget and its evolution over time.

6.3.3.1 Atmospheric Changes

Since the beginning of the Industrial Era, the atmospheric CH_4 concentration increased by a factor of 2.5 (from 722 ppb to 1803 ppb in 2011). CH_4 is currently measured by a network of more than 100 surface sites (Blake et al., 1982; Cunnold et al., 2002; Langenfelds et al., 2002; Dlugokencky et al., 2011), aircraft profiles (Brenninkmeijer et al., 2007), satellite (Wecht et al., 2012; Worden et al., 2012) and before 1979 from analyses of firn air and ice cores (see Sections 5.2.2 and Section 6.2, and Figure 6.11). The growth of CH_4 in the atmosphere is largely in response to increasing anthropogenic emissions. The vertically averaged atmospheric CH_4 concentration field can be mapped by remote sensing from the surface using Fourier Transform Infrared Spectroscopy (FTIR) instruments (Total Carbon Column Observing Network, TCCON, http://www.tccon.caltech.edu/) and from space by several satellite instruments: Atmospheric Infrared Sounder (AIRS, since 2002; http://airs.jpl.nasa.gov), Tropospheric Emission Spectrometer (TES, since 2004; http://tes.jpl.nasa.gov), Infrared Atmospheric Sounder Interferometer (IASI, since 2006; Crévoisier et al., 2009), Scanning Imaging Spectrometer for Atmospheric Cartography (SCIAMACHY, 2003–2012; Frankenberg et al., 2008), and Greenhouse Gases Observing Satellite-Thermal And Near infrared Sensor for carbon Observation Fourier-Transform Spectrometer (GOSAT-TANSO-FTS, since 2009; Morino et al., 2011). As an example, SCIAMACHY shows the column CH_4 gradient between the two hemispheres as well as increased concentrations over Southeast Asia, due to emissions from agriculture, wetlands, waste and